



Investigation of using the ceramic polishing brick powder in engineered cementitious composites

Yan Xiong ^{a,b}, Guozhong Xu ^a, Di Wu ^{c,*}, Shuai Fang ^a, Yingfeng Tang ^d

^a School of Civil Engineering and Transportation, South China University of Technology, Guangzhou, China

^b State Key Laboratory of Subtropical Building Science, South China University of Technology, Guangzhou, China

^c Earthquake Engineering Research and Test Center, Guangzhou University, Guangzhou, China

^d Guangzhou Pearl River Foreign Investment Architectural Design Institute Co. Ltd, Guangzhou, China



ARTICLE INFO

Keywords:

Ceramic polishing brick powder
Engineered cementitious composites
Uniaxial tensile
Axial compression
Activity index
Pore structure

ABSTRACT

With the development of the ceramic industry and the renovation of old buildings, ceramic waste is increasing dramatically in the process of production. Among ceramic wastes, ceramic polishing brick powder (CPBP) has high hardness and a large amount of silicate minerals, which endow it with a good skeleton and pozzolanic activity. Therefore, reasonable recycling of CPBP has important environmental protection and economic values. This study used CPBP as a supplementary cementing material to replace fly ash in engineered cementitious composites (ECCs). The basic characteristics of CPBP were characterized by an activity index test and micro analysis for comparison with fly ash. Prior to the uniaxial tensile test of the newly designed ECC, an axial compression test, X-ray diffraction (XRD), and mercury intrusion porosimetry (MIP) of cement quartz mortar (CQM) were conducted to evaluate the feasibility of replacing fly ash with CPBP in ECCs. The test results show that the fineness of CPBP is between that of cement and fly ash, and that CPBP particles have a smoother surface than cement particles. The 7-day activity index of CPBP was the same as that of fly ash, while the 28-day activity index of CPBP was 14.29% higher. When the CPBP content is 35% of the cementitious material, the compressive and tensile strengths of CQM are maximized. The addition of CPBP significantly decreased the porosity and achieved pore structure refinement of CQM. When CPBP replaces half or all fly ash, the newly designed ECC can achieve good tensile properties. Moreover, by replacing fly ash with CPBP at 35% of the cementitious material, the designed ECC specimen showed a better tensile strength (5.89 MPa) and ultimate tensile strain capacity (4.39%). Therefore, it has great engineering application prospects.

1. Introduction

In recent years, the development of the ceramic industry and the reconstruction of old buildings have resulted in considerable waste [1]. Ceramic waste is both construction and industrial waste. Part of the ceramic waste comes from old tiles or sanitary ware produced by the demolition of old buildings [2–4], while other part comes from the manufacture of ceramic products [5–8]. China is the largest producer and seller of ceramics worldwide. In 2017, the annual production of ceramic tiles in China was 10.15 billion square meters, and the export of ceramic tiles was 821 million square meters, and both were ranked first in the world [9]. The Association of Italian Manufacturers of Machinery and Equipment for the Ceramic Industry (ACIMAC) [10] reported that in

2018 the production of tiles worldwide was approximately 13.7 billion m². As the production rate of ceramic products increases, the amount of ceramic waste generated during production and processing increases. Typically, approximately 30% of the overall production of the local ceramic industry is wasted [11,12]. At present, the treatment and recycling rates of ceramic waste are relatively low in China. Vast quantities of these ceramic wastes are being dumped in open-air stacking or landfills, which occupy cultivable land and pollute the environment. It is necessary to find an alternative to the discarding of ceramic wastes able to promote the effective recycling of resources, reduce waste accumulation, and generate significant economic and environmental benefits.

Previous research [13–15] has mentioned that ceramic wastes have

* Corresponding author.

E-mail addresses: xyan@scut.edu.cn (Y. Xiong), 1126917105@qq.com (G. Xu), wudiwdzoo@gmail.com (D. Wu), fangshuai@scut.edu.cn (S. Fang), tangyf@pearl-river.com (Y. Tang).

great potential for the preparation of recycled aggregates and additives. Torkittikul and Chaipanich [16] used ceramic wastes as fine aggregates of Portland cement and fly ash concretes. The compressive strength of ceramic waste concrete was found to increase with ceramic waste content and was optimum at 50% for the control concrete; the compressive strength of the fly ash concrete increased with increasing ceramic waste content up to 100%. Alves et al. [17] pointed out that recycled ceramic fine aggregates are suitable for concrete as a natural fine aggregate replacement in terms of compressive and tensile strength. Serkan et al. [18] reported that waste ceramic powders (CPs) have the potential to be used in self-consolidating concretes (SCCs) as cement replacement, up to 15%, and to improve the flowability and passing ability of fresh SCCs. Samadi et al. [19] evaluated the mechanical properties and durability of a mortar comprising ceramic waste as supplementary cementitious material and ceramic particles as fine aggregates and showed that the use of ceramic waste as both a cement replacement and fine aggregates significantly improved the compressive strength, durability performance, and sulfate resistance capacity of the mortar. Ceramic wastes contain most of the sludge generated during the ceramic polishing process, particularly ‘porcellanato’ and ‘monoporosa’, which are rich in silica (SiO_2) and alumina (Al_2O_3) with good pozzolanic activity [20]. Steiner et al. [21] investigated the synergistic effect of ‘porcellanato’ and ‘monoporosa’ polishing residues (MixPR) as supplementary cementitious materials and reported that the mortar compositions using MixPR maintained their plasticity and showed a high pozzolanic activity index. The 28-day compressive strength of mortar compositions decreased with increasing amounts of MixPR, but the compressive strength of a mortar composition using 25% MixPR at 120 days was higher than that of mortar without MixPR. Li et al. [22] investigated the workability, strength, and microstructure of trial mortar mixes at various water/cement ratios and ceramic polishing waste (CPW) volumes and found that with up to 20% CPW added as paste replacement, the cement content could be reduced by 33%, the 7-day and 28-day cube strengths could be increased by at least 85%, and the microstructure could be densified. In the following year, Li et al. [23] continued to test the workability, compressive strength, and chloride resistance of mortar mixes with different ceramic polishing residue (CPR) contents and showed that adding up to 20% CPR to replace cement always increased the 28-day cube strength and chloride resistance.

Engineered cementitious composites (ECCs) are designed based on a micromechanical model by rationally controlling the fiber, matrix, and fiber/matrix interface properties [24]. ECCs can exhibit strain-hardening properties with an ultimate tensile strain exceeding 4% at a moderate fiber volume fraction of 2.0% [25]. ECCs have high toughness, tensile strength, fracture resistance, and multi-cracking characteristics. In addition, ECCs have shown excellent performance in terms of bending, compression, and other basic mechanical properties [25–30], and have been applied in several projects. Half the depth of the asphalt overlay on the steel deck of the Mihara Ohashi bridge was replaced with a 40 mm thick fiber reinforced cementitious composite to improve the fatigue resistance of the stiffener for the steel deck [31]. An ECC was used in the bridge deck link slabs of an ECC-concrete bridge deck in southeast Michigan, USA [32].

The ECC mainly consists of cement, mineral additive, fine aggregates, water, and admixtures that are used to enhance its strength and workability, with no more than 2% volume of short fibers [34]. With the development of the construction industry, a large amount of ordinary Portland cement is used as a binder material for preparing concrete. Furthermore, the ECC does not contain coarse aggregates according to the micromechanical design model; it consumes a relatively higher amount of cement than conventional concrete. The production of ordinary Portland cement requires many natural resources, consumes much energy, and releases large amounts of carbon dioxide to the environment, causing a series of environmental pollution problems [35]. Using mineral admixtures from industrial byproducts or waste as a replacement for Portland cement, the preparation of new green cement-based

composite materials is a critical step in ensuring the construction industry's sustainability. Pan et al. [34] proposed an ECC mix with fly ash as a 70% cement replacement, which presents a suitable strain hardening property. However, as common mineral additives, low-quality fly ash will hurt the workability and mechanical properties of concrete, while high-quality fly ash is insufficient in supply and has a high price [36]. As mentioned above, ceramic waste, as a sustainable and easily available material, has great potential for replacing cement or fly ash in ECC materials. Zhao et al. [33] used CP as a supplementary cementing material to partially replace cement in PVA-ECC materials and pointed out that when the content of fly ash (FA) is 70%, the content of cement is 10%, and the content of solid waste CP is 20%, the ECC material achieves the largest uniaxial tensile strain of 4.94%. However, to the best of our knowledge, there is limited literature on the mechanical properties of ECCs containing ceramic polishing brick powder as both a cement and fly ash substitute.

Thus, in this study, new types of ECC were prepared by incorporating CPBP as a cementitious admixture instead of fly ash. Owing to the precise design of ECCs, the mechanical properties and microstructure of the matrix directly affect the ECC performance. The basic characteristics of CPBP and CQM were first investigated, and the feasibility of using CPBP as a substitute for fly ash was verified by a uniaxial tensile test.

2. Materials and methods

2.1. Materials

The ECC was made of cement, fly ash, CPBP, quartz sand, and water. The P-O 42.5R ordinary Portland cement was produced by Guangzhou Shijing Cement Company. The fly ash was Grade I Class F fly ash from Longze Water Purification Material Co. Ltd, with a water content of 0.21% and a specific surface area of 362 m^2/kg . The CPBP in this test was collected during the production process of ceramic tile products, such as screeding, grinding, and polishing. The chemical compositions of the raw materials were tested using X-ray fluorescence (XRF) spectrometry, as presented in Table 1. Quartz sand was required to pass through a 100 mesh sieve with a mean particle size of 142 μm . The main components of the CPBP were SiO_2 and Al_2O_3 , and its chloride ion content was less than 0.06%, which meets the requirements of GB/T 51,003–2014 [37]. A polycarboxylic superplasticizer (SIKA Viscocrete 20HE-40) was used to improve the workability of the ECC and reduce the water requirement. Polyvinyl alcohol (PVA) fiber from Kuraray Co. Ltd. (Osaka, Japan) was used at a volume fraction of 2%. The properties of the PVA fibers are listed in Table 2.

2.1.1. Particle size distribution

The particle size of cementitious materials such as cement, fly ash, and CPBP has a significant influence on the characteristics of cement mortar or concrete, which mainly include strength, workability, and microstructure [38–41]. The particle size of the raw materials was tested using the wet dispersion technology with a laser diffraction particle size analyzer according to the requirements of ISO 13320-1-1999 [42]. Ultrasonic high-frequency vibration was used to fully disperse the

Table 1
Chemical composition of raw materials (%).

Raw Materials	Cement	Fly Ash	CPBP
SiO_2	19.57	53.97	69.04
Al_2O_3	7.69	31.15	16.92
CaO	59.21	4.01	1.43
Fe_2O_3	2.39	4.16	0.77
MgO	2.84	1.01	1.38
Na_2O	–	0.89	2.17
K_2O	0.59	2.04	2.17
SO_3	2.45	0.73	–
Cl	0.01	0.01	0.05

Table 2

Properties of PVA fiber.

Fiber type	Diameter (μm)	Length (mm)	Aspect ratio	Tensile strength (MPa)	Elongation (%)	Elastic modulus (GPa)	Density (kg/m^3)
PVA	40	12	300	1560	6.5	41	1300

agglomerated particles, and the electromagnetic circulation pump evenly distributed the small and large particles throughout the circulation system, thereby fundamentally ensuring the accurate repetition of the wide distribution sample test. Fig. 1 illustrates the particle size distributions of cement, fly ash, and CPBP. As can be observed, the particle size distributions of cement, CPBP, and fly ash are mainly in the range of 10–20 μm . The median particle sizes of cement, CPBP, and fly ash are 11.56, 12.73, and 15.05 μm . The cement fineness is the minimum, followed by that of CPBP, and the fineness of the fly ash is the largest. The mean particle size of CPBP is smaller than that of the fine aggregate, and thus, the CPBP could be used to fill the voids between the aggregate particles [22]. The particle distribution of cement was relatively concentrated, and the maximum particle size did not exceed 45 μm . In contrast, there were more larger particles in the fly ash and CPBP samples. The particle sizes of fly ash and CPBP were similar, and the CPBP was slightly finer than fly ash.

2.1.2. Loss on ignition and sieve residue

Loss on ignition and sieve residue are important indicators for evaluating the quality of cementitious materials. According to GBT 176–2017 [43], the loss on ignition of materials was calculated by measuring the mass of samples before and after burning at 1000 °C in a high-temperature furnace. The 45 μm sieve residue of the samples was tested using a FSY-150E cement fineness negative pressure screen analyzer in conformity with the requirements of GBT 51003–2014 [37]. The loss on ignition and 45 μm sieve residue of each mineral additive are presented in Table 3. According to the requirements for the loss on ignition of materials in Refs. [44,45], the loss on ignition of PO cement and Grade I Class F fly ash should be $\leq 5.0\%$. In this test, fly ash met the requirements. At present, there is no requirement for the loss of ignition of the CPBP, and the loss of ignition of CPBP used in this experiment was $\leq 3.0\%$, which meets the requirements of PO cement and Grade I Class F fly ash. According to the guidelines indicated in GBT 1596–2017 [45], Grade I Class F fly ash requires $\leq 12.0\%$ sieve residue. The fineness of the fly ash meets this requirement, and other cementitious materials have no clear regulations. From the test results, the 45 μm sieve residue of the CPBP used in this experiment was 3.1%, which was the smallest among the mineral additives.

2.1.3. Micro-morphology

The micro-morphology of the raw materials was observed using scanning electron microscopy (SEM). The test procedure can be divided

Table 3

Loss on ignition and sieve residue test results.

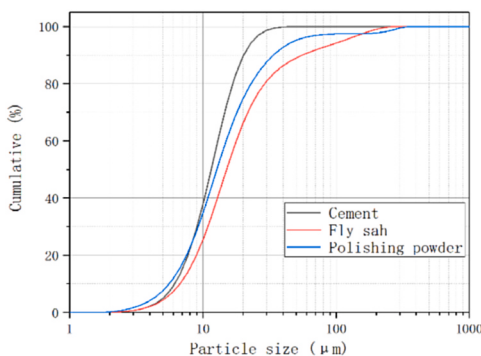
Sample	Cement	Fly ash	CPBP
Average of loss on ignition	3.20%	4.66%	2.93%
Sieve residue	10.2%	10.7%	3.1%

into four steps: 1) Five samples were placed in a 105 °C blast drying oven and dried for 2 h to a constant weight. After the samples were cooled, they were placed in sealed bags; 2) a double-sided conductive adhesive pasted the sample on the sample stage in the scanning room, the sample stage was gently tapped to clean up the excess sample and ensure that the sample did not easily drop; and 3) before carrying out the electron microscope test, the sample stage with the sample was placed in the vacuum etching coating instrument to high-pressure spray gold. It took approximately 5 min to ensure that a certain thickness of the conductive film was formed on the surface of the sample, so that better images were obtained in the test. After that, the sample preparation was completed; 4) finally, the sample was placed in the SEM instrument for detection.

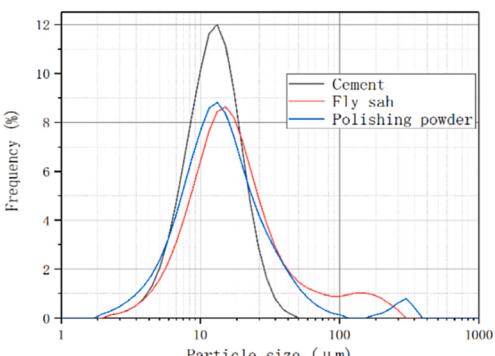
Fig. 2 shows SEM images of each cementitious material. As shown in Fig. 2, the microscopic morphology of fly ash is quite different from those of cement and CPBP. The particles of cement and CPBP were irregularly shaped particles. CPBP particles have a smoother surface than cement particles because CPBP is produced by polishing. The CPBP roughness and elongation are small, and its particle shape can play a specific role in filling and deflocculating, and improving the fluidity of the matrix [15]. The particles of fly ash have a distinct spherical shape; thus, the cement-based mixture with fly ash presents good fluidity and low water requirements. The CPBP can be in a good dispersion state in the cement paste and helps to fill and refine the pores of the hardened paste, making the particle accumulation of the system more compact and reasonable, thereby improving the workability of the mortar mixing and the structure of the hardened mortar [16].

2.2. Methods

The activity index of fly ash and CPBP was evaluated using the mineral admixture activity index test method specified in GBT 51003–2014 [37]. The flexural strength, compressive strength, workability, and activity index of cement mortar with fly ash and CPBP as mineral additives were tested. After measuring the mortar's compressive



(a) Cumulative particle size



(b) Particle size frequency

Fig. 1. Distribution of particle size and frequency.

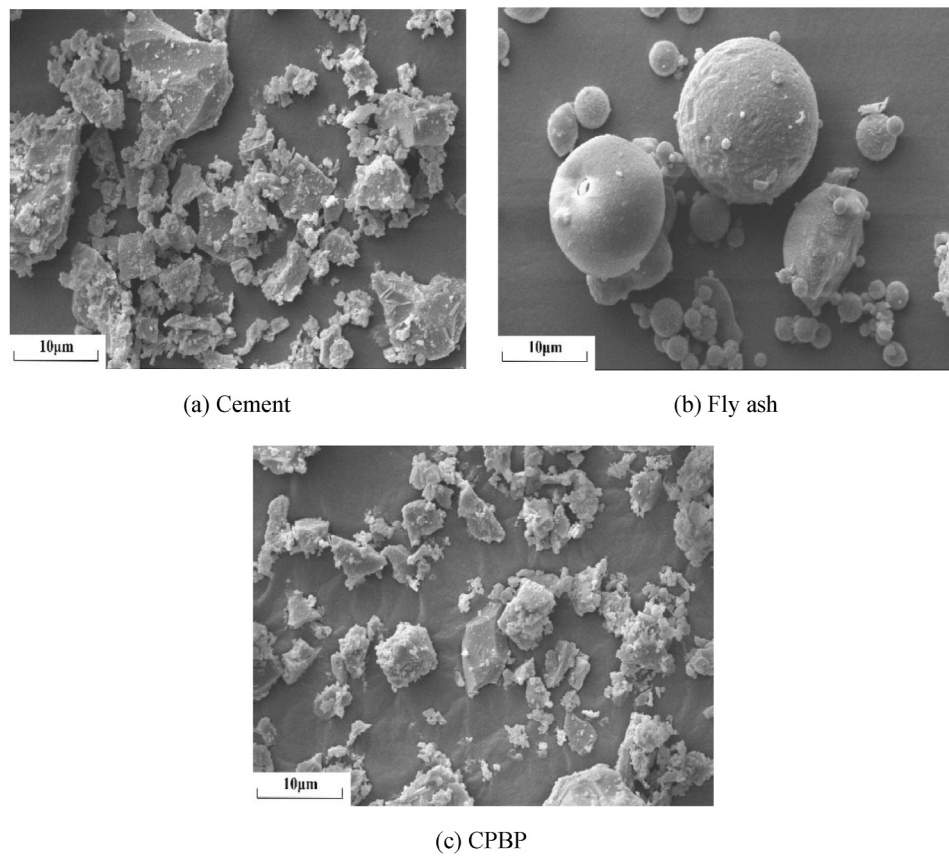


Fig. 2. Microscopic morphology.

strength at the predetermined curing age, the activity index of the mineral additive was calculated using the following formula, and the integer part of the calculation result was regarded as the activity index.

$$A = \frac{R_t}{R_0}$$

where A is the activity index of the mix (%), R_t is the compressive strength of the tested mortar that contains 50% admixture (MPa), and R_0 is the compressive strength of the reference mortar (MPa).

To measure the flexural strength of the hardened mortar, three prism specimens at each age group were produced with a standard prismatic dimension of 40 mm × 40 mm × 160 mm according to the requirements of GB/T17671-1999 [42]. The specimens were produced by JJ-5 planetary cement mortar mixers and cured until the predetermined ages (7 days and 28 days). A compression test was performed on the broken prism. The compression surfaces were the two sides of the specimen, each one with an area of 40 mm × 40 mm. A 20-ton universal testing machine was used for the flexural strength and compression tests, which were conducted with loading rates of 50 and 1500 N/s. The average test results from triplicate flexural strength and sextuplicate compression strength tests of the specimens were recorded for each mix. The fluidity of the cement mortar was determined using a table jumping test referenced in GB/T 2419-2005 [46].

The mixture proportion of the mineral admixture activity index test is tabulated in **Table 4**, where the ISO sand meets the requirements of standards [47,48]. The test specimens were divided into five groups, where C, F, and P indicate the cement, fly ash, and CPBP, respectively. As a control group, C-0 indicates cement mortar without any mineral additives. C-F30 and C-F50 represent cement–fly ash mixed mortars obtained by replacing part of the cement with fly ash, whereas C-P30 and C-P50 represent the mortar mixed with CPBP to replace part of the cement. The number in the name of each group indicates the

Table 4
Mixing ratio of activity index test.

Sample	Cement/g	Fly ash/g	CPBP/g	ISO sand/g	Water/g
C-0	450	0	0	1350	225
C-F30	315	135	0	1350	225
C-F50	225	225	0	1350	225
C-P30	315	0	135	1350	225
C-P50	225	0	225	1350	225

replacement ratio of fly ash and CPBP.

This study referred to related research [34,49,50], designed the ECC mix proportions according to the workability, and obtained the mix proportions, as listed in **Table 5**. As presented in **Table 5**, F is the fly ash, and P is CPBP. F70 indicates that fly ash accounts for 70% of the total mass fraction of cementitious materials. FP35 means that fly ash and CPBP account for 35% of the total cementitious material mass fraction, respectively. Cement quartz mortar (CQM) refers to the ECC mix proportions, excluding fiber. The water–binder ratio and sand–binder ratios of the examples are 0.35 and 0.33, respectively, and the volume of PVA fiber is 2.0%. By adjusting the amount of superplasticizer, the fluidity of the ECC examples is maintained at approximately 200 mm. The actual SP dosage needed was determined by carrying out mortar mixing trials with the mass of liquid SP as a percentage of the mass of cementitious materials. A uniaxial tensile test, axial compression test, mercury intrusion porosimetry (MIP), and X-ray diffraction (XRD) tests were conducted to characterize the tensile behavior and microscopic features of CQM (without any fibers). More detailed steps of the tests can be found in Ref. [51]. The tensile properties of the designed ECC were investigated by a uniaxial tensile test. For each CQM mix proportion, three A 70.7 × 141.4 mm cylindrical pieces were made for the axial compression test and three pieces for the static compression elastic

Table 5Mix proportions of samples (kg/m^3).

Component	Cement	Fly ash	CPBP	Quartz sand	Water	Superplasticizer	Thickener	PVA
F70	323.21	754.17	0	355.54	371.91	6.47	0.54	26
F70 CQM	323.21	754.17	0	355.54	371.91	6.47	0.54	0
FP35	323.21	377.08	377.08	355.54	369.00	10.11	0.54	26
FP35 CQM	323.21	377.08	377.08	355.54	369.00	10.11	0.54	0
P70	323.21	0	754.17	355.54	365.00	15.10	0.54	26
P70 CQM	323.21	0	754.17	355.54	365.00	15.10	0.54	0

modulus test. Six dog-bone-type specimens were subjected to uniaxial tensile tests for each mix proportion. Each test takes the average of all the specimen results as the final result. The specific dimensions of the dog-bone-type specimen are shown in Fig. 3. The uniaxial tensile and axial compression tests were conducted following references [47,52,53]. These tests were controlled in an electrohydraulic servo tester at a loading rate of 0.5 mm/min. To measure the deformation during loading, two LVDTs were installed in the middle of the specimens, with a gauge length of 80 mm for the tensile test specimens and of 70.7 mm for the axial compressive test specimens. In this study, two U-shaped chucks were designed to clamp both ends of the specimen, and two U-shaped chucks were connected to the test machine through a spherical hinge. When the specimens were installed, attention was paid to the alignment between the central axis of the specimen and the testing machine, and it was ensured that the alignment between chucks in the test machine was properly vertical. The loading beam of the testing machine was slowly raised so that the specimen could be stably clamped for loading and data collection. Fig. 4 shows a schematic of these tests.

3. Results and discussion

3.1. Activity index test

The results of the activity index tests are presented in Table 6. Figs. 5 and 6 show the flexural strength and compressive strength of each group sample, respectively. The age and type of the mineral additive significantly influenced the flexural strength and compressive strength of the cement mortars. At the age of 7 days, the control group C-0 presented the highest flexural strength and compressive strength among the samples, and the flexural and compressive strengths of the cement mortars decreased as the proportion of mineral additive increased. The flexural and compressive strengths of C-P30 were reduced by 12.82% and 25.08%, respectively, compared with those of C-0, and they were reduced by 6.85% and 13.21%, respectively, compared with those of C-F30. The flexural and compressive strengths of C-P50 decreased by



(a) Uniaxial tensile test (b) Axial compression test

Fig. 4. Test schematic diagram.

Table 6

Activity index test results.

Sample	Flexural Strength/MPa		Compressive Strength/MPa		Activity Index		Fluidity/mm
	7 days	28 days	7 days	28 days	7 days	28 days	
C-0	7.8	9.6	30.7	42.0	100	100	129
C-F30	7.3	8.6	26.5	38.0	86	90	145
C-F50	5.0	7.4	17.0	29.3	55	70	146
C-P30	6.8	8.4	23.0	38.1	75	91	133
C-P50	5.4	8.4	16.9	33.5	55	80	125

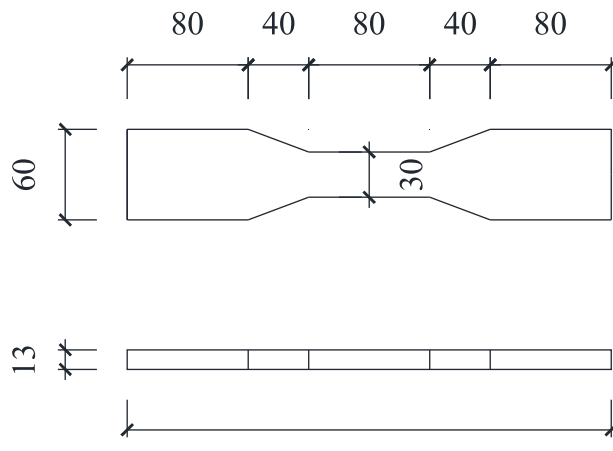


Fig. 3. Specific dimensions of examples (mm).

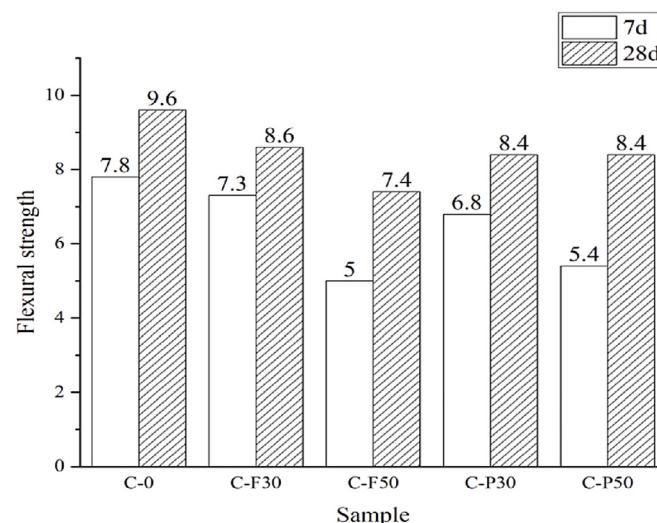


Fig. 5. Flexural strength of each sample.

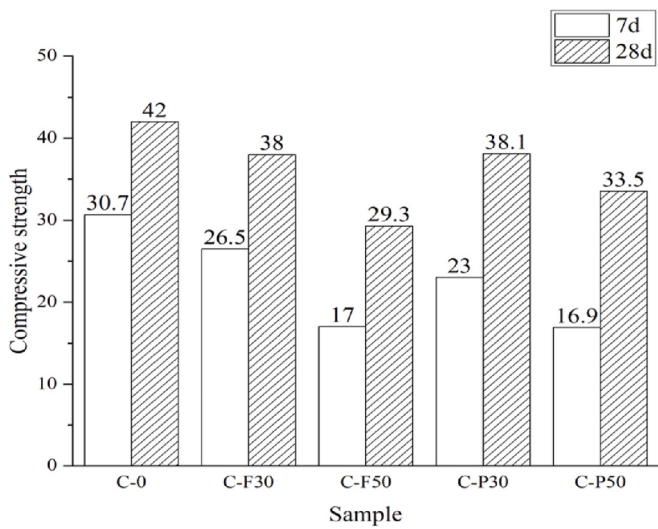


Fig. 6. Compressive strength of each sample.

30.77% and 44.95%, respectively, compared with those of C-0, and increased by 8.00% and decreased by 0.59% compared with those of C-F50. When the age increased to 28 days, the flexural and compressive strengths of C-P30 decreased by 12.50% and 9.29%, respectively, compared to those of C-0. Compared to C-F30, the flexural strength of C-P30 was reduced by 2.33% and the compressive strength of C-P30 increased by 0.26%. The flexural and compressive strengths of C-P50 were reduced by 12.50% and 20.24%, respectively, compared with those of C-0, whereas they increased by 13.51% and 14.33%, respectively, compared to those of C-F50.

The test results showed that the amount of CPBP had a significant effect on the flexural strength and compressive strength of the cement matrix at the age of 7 days, and it had a particular effect on the compressive strength but had no effect on the flexural strength of the cement matrix at the age of 28 days. The flexural and compressive strengths of C-F30 and C-F50 containing fly ash were very close to those of C-P30 and C-P50 containing CPBP at the age of 7 days. When the age increased to 28 days, there was a significant difference in the growth rate between the flexural and compressive strengths of the specimens with fly ash or CPBP. The growth rates of the flexural and compressive strengths of the specimens with CPBP were greater than those of the specimens with fly ash.

Fig. 7 shows the activity indices of each sample. In this test, CPBP had the highest activity index, followed by fly ash. At the age of 7 days, the activity index of CPBP was the same as that of fly ash. However, with an increase in age, the activity index of CPBP gradually approached that of fly ash. At 28 days of age, the activity index of CPBP was 14.29% higher than that of fly ash.

Fig. 8 shows the fluidity of each specimen. The fluidity of the specimens with different types and addition of mineral additives varied greatly. C-F30 and C-F50 had higher flow expansion than C-P30, C-P50, and C-0, because the fly ash particles have a distinct spherical shape and a lubricating effect, which makes the mixture of fly ash have a higher fluidity. The fluidity of C-P30 was greater than that of C-P50. Thus, it can be inferred that adding a certain amount of CPBP improves the fluidity of CQM.

3.2. Compressive properties of CQM

The axial compressive properties of the tested CQM cylindrical samples are presented in Fig. 9, where E_c is the elastic modulus under axial compression. As shown in Fig. 9, when the content of CPBP increased from 0% in the F70 CQM to 35% in the FP35 CQM, the axial compressive strength of CQM increased by 35.9%. However, within the

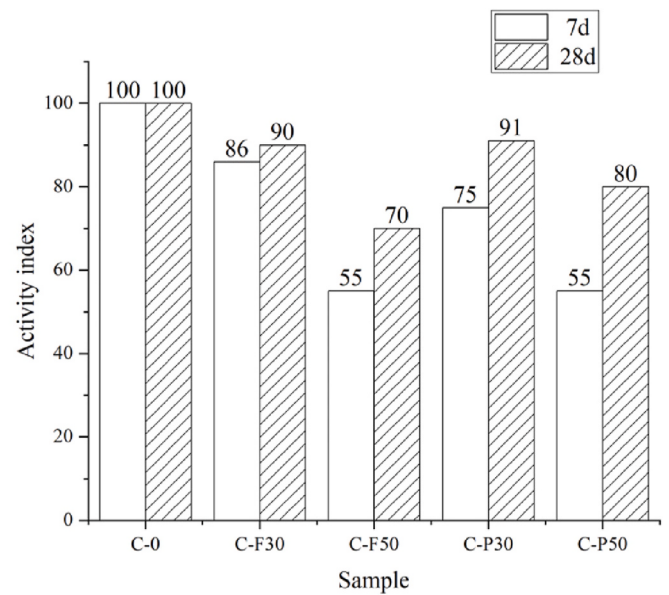


Fig. 7. Activity index of each sample.

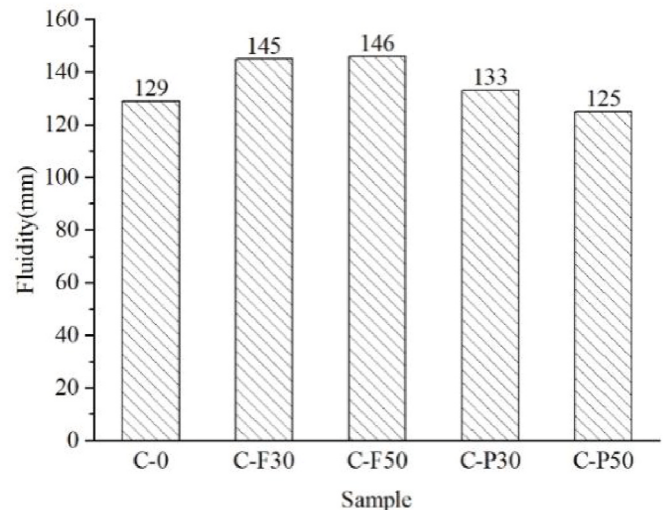


Fig. 8. Fluidity of each sample.

range of CPBP content from 35% to 70%, the compressive strength of CQM increased slightly. During this process, the elastic modulus of CQM continued to increase. As the CPBP content increased, the axial compressive strength of CQM increased and finally stabilized, while the elastic modulus continued to increase. In other words, when CPBP replaced 35% of fly ash, the axial compressive strength of the ECC was maximized in this test. The increase in the CPBP content reduced the ultimate compressive strain of CQM. When the CPBP content increased from 0% to 35% and from 35% to 70%, the ultimate compressive strain of CQM decreased by 7.4% and 11.5%, respectively. Combined with the changing trend of the axial compressive strength, it can be inferred that the recommended dosage of CPBP replacing fly ash should not exceed 35%.

The stress-strain curves of the tested cylinder samples under compression are shown in Fig. 10. In general, the curves can be divided into three stages: the rising stage of elastic deformation, the plastic deformation stage, and the falling stage after the peak load. However, because there were no coarse aggregates and fibers, the CQM quickly formed obvious vertical cracks after reaching the limit state and failed.

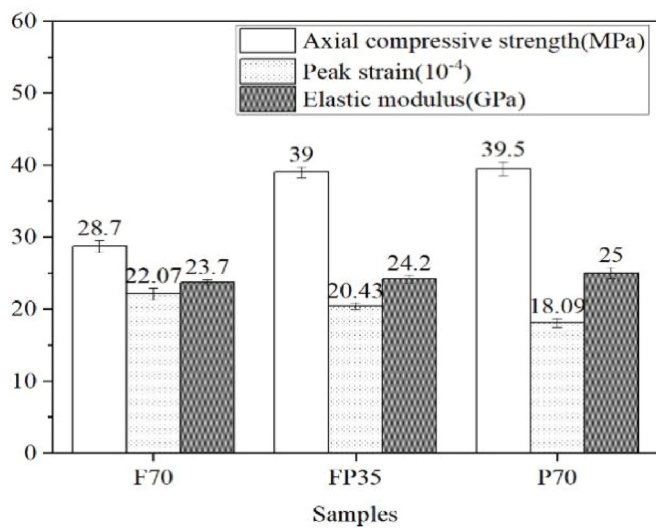


Fig. 9. Axial compressive properties of CQM.

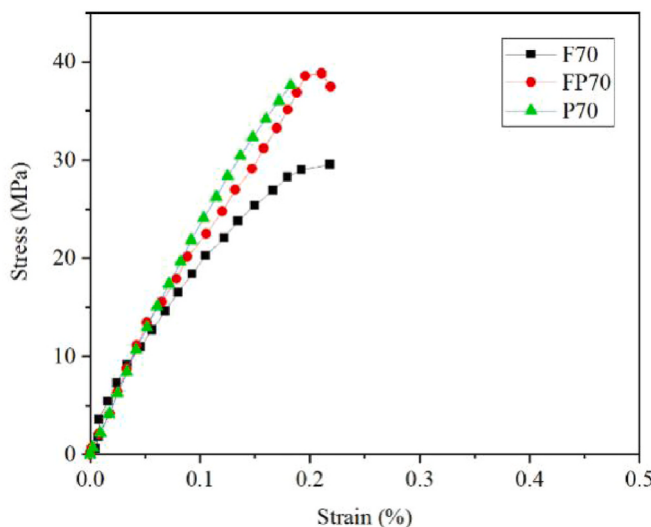


Fig. 10. Axial compressive stress-strain curves of CQM.

Fig. 11 shows the failure states of the specimens.

3.3. Tensile properties of CQM

The uniaxial tensile test results of CQM at 28 days of age are summarized in Fig. 12, and the tensile stress-strain curves are shown in Fig. 13. E_t is the elastic modulus under uniaxial tensile load. The results showed that CQM exhibited obvious brittleness during uniaxial tensile loading. As the content of CPBP increased from 0% in F70 to 35% in FP35, the tensile strength and elastic modulus of CQM increased by 6.3% and 12.0%, respectively. When the CPBP content increased from 35% to 70%, CQM did not increase in tensile strength, and the trend was similar to that of the axial compressive strength of the cylinder samples. FP35 CQM and F70 CQM have similar ultimate tensile deformation capacities, but the ultimate strain of FP70 CQM was 14.5% lower than that of F70 CQM. It can be observed that with the increase in CPBP replacing fly ash, the tensile strength and elastic modulus of CQM increase. Among them, the tensile elastic modulus of CQM increased faster, while the ultimate tensile strength changed less.

3.4. XRD analyses

The results of the compressive and tensile tests of CQM showed that the influence of the content of CPBP replacing fly ash on the compressive and tensile properties of CQM was monotonous. To understand the

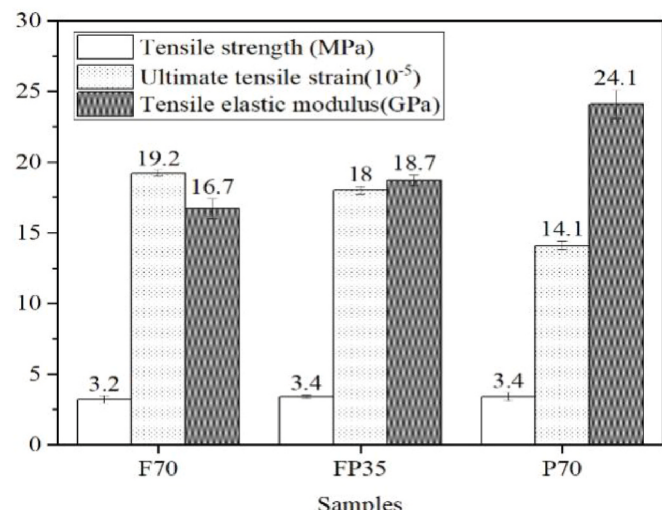


Fig. 12. Tensile properties of CQM.

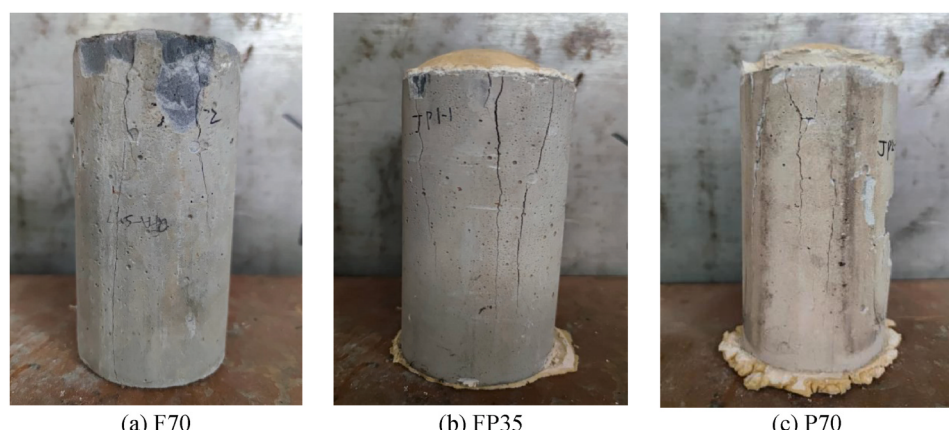


Fig. 11. Failure state of CQM.

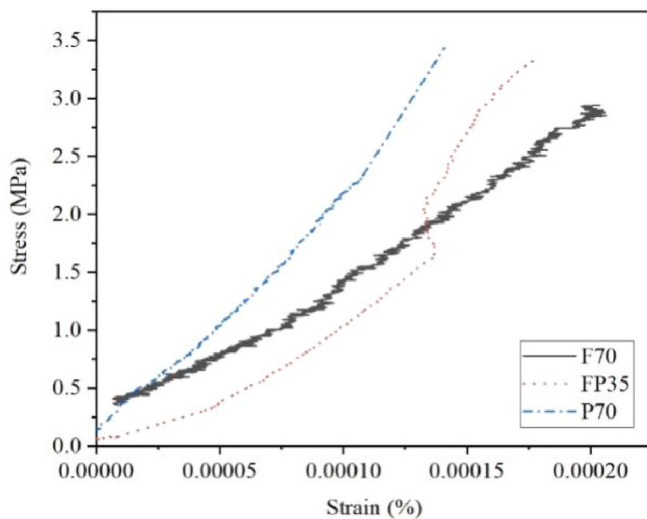


Fig. 13. Tensile stress–strain curves of CQM.

influence of a certain additive on CQM more intuitively, XRD analyses were performed on the F70 and P70 CQM specimens. The main mineral of CPBP is quartz, which also contains a certain amount of calcium silicate hydrate and calcium aluminate hydrate. The main mineral of fly ash is quartz, followed by mullite [15,54,55]. The test results are shown in Fig. 14, and the mullite and silica can be observed in the XRD pattern of the F70 CQM at the ages of 28 days and 90 days, indicating that these two phases do not participate in the hydration reaction. In the F70 CQM, a visible calcium hydroxide peak appeared at 28 days, and as the age increased to 90 days, the calcium hydroxide peak disappeared and was replaced by the monosulfide hydrated calcium sulfoaluminate peak, which is the product of the hydration of tricalcium aluminate and ettringite. During this period, the peaks of calcite increased significantly, and the crystallinity increased; thus, it can be inferred that calcite is one of the hydration products. As shown in Fig. 14(b), when the P70 matrix's age reached 90 days, the sodium thiosulfate peak disappeared, and the peaks of magnesium carbonate, andradite, and calcium orthosilicate appeared in the XRD pattern of P70 CQM. Compared with F70 CQM, there was no calcium hydroxide peak but a calcium carbonate peak in the P70 CQM at 28 days. The active SiO₂ in CPBP participates in hydration to a greater extent than fly ash, which produces more compounds that significantly contribute to the strength and benefits the matrix's early strength growth [56].

3.5. Pore structure analyses

The material's macroscopic mechanical properties, including

strength and stiffness, are closely related to the pore structure of the material [57]. To further explore the influence of a certain additive on CQM, the pore structure parameters of the F70 and P70 CQM after standard curing for 28 days are listed in Table 7. The porosity of the P70 CQM at 28 days was 13.95% lower than that of F70 CQM. The total pore volume decreased by 27.12%, the total pore area decreased by 9.58%, and the average pore size decreased by 19.32%. The most probable pore size was the most obvious, with a decrease of 58.13%. The reduction in the most probable pore size indicates that the addition of CPBP helps to refine the pore structure of CQM [56]. The median pore size of P70 CQM increased by 32.95%. The test results show that CPBP can significantly refine the CQM pore structure, mainly because the fineness of CPBP is higher than that of fly ash, and its activity index is higher than that of fly ash. The replacement of fly ash with CPBP promotes the hydration reaction, produces more hydration products, and has a better pore filling effect in CQM. This result was also found in the XRD analysis of CQM. Therefore, the pore structure of CQM becomes denser as CPBP replaces fly ash.

The pore size distribution diagram of each sample is shown in Fig. 15. According to the pore size, the pore structure can be divided into four levels: gel pores (diameter: < 10 nm), transition pores (diameter: 10–100 nm), capillary pores (diameter: 100–1000 nm), and macropores (diameter: > 1000 nm) [58], where pore diameters > 100 nm are harmful pores [59].

As can be observed from Fig. 15, the pore size distribution curve of P70 CQM inside the cement matrix obviously moves to the left compared to that of F70 CQM, and the number of harmful pores larger than 100 nm decreased significantly after replacing fly ash with CPBP. The pore size of F70 CQM is mainly distributed in the range of 10–80 nm, and the most probable pore size is mainly distributed between 30 and 50 nm. The pore size of P70 CQM is mainly distributed in the range of 10–30 nm, and the most probable pore size is mainly distributed in the range of 10–20 nm.

3.6. Tensile properties of ECC

The uniaxial tensile test results and tensile properties of the ECC at

Table 7

Pore structure parameters of each CQM sample.

Pore structure parameter	Sample	
	F70 CQM	P70 CQM
Total pore volume (mL/g)	0.2316	0.1688
Total porosity (%)	32.97	28.37
Median pore diameter (nm)	8.8	11.7
Average pore size (nm)	20.7	16.7
Total pore area (m ² /g)	44.786	40.496
Most probable pore size (nm)	50.34	21.08

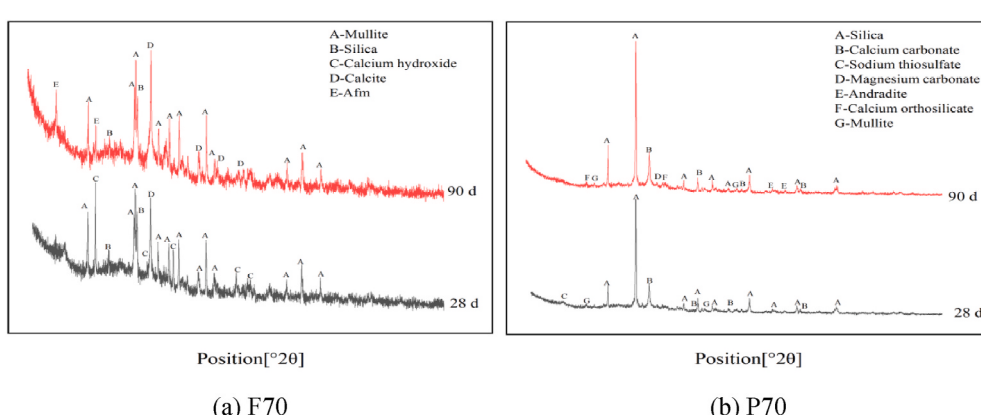


Fig. 14. XRD of CQM

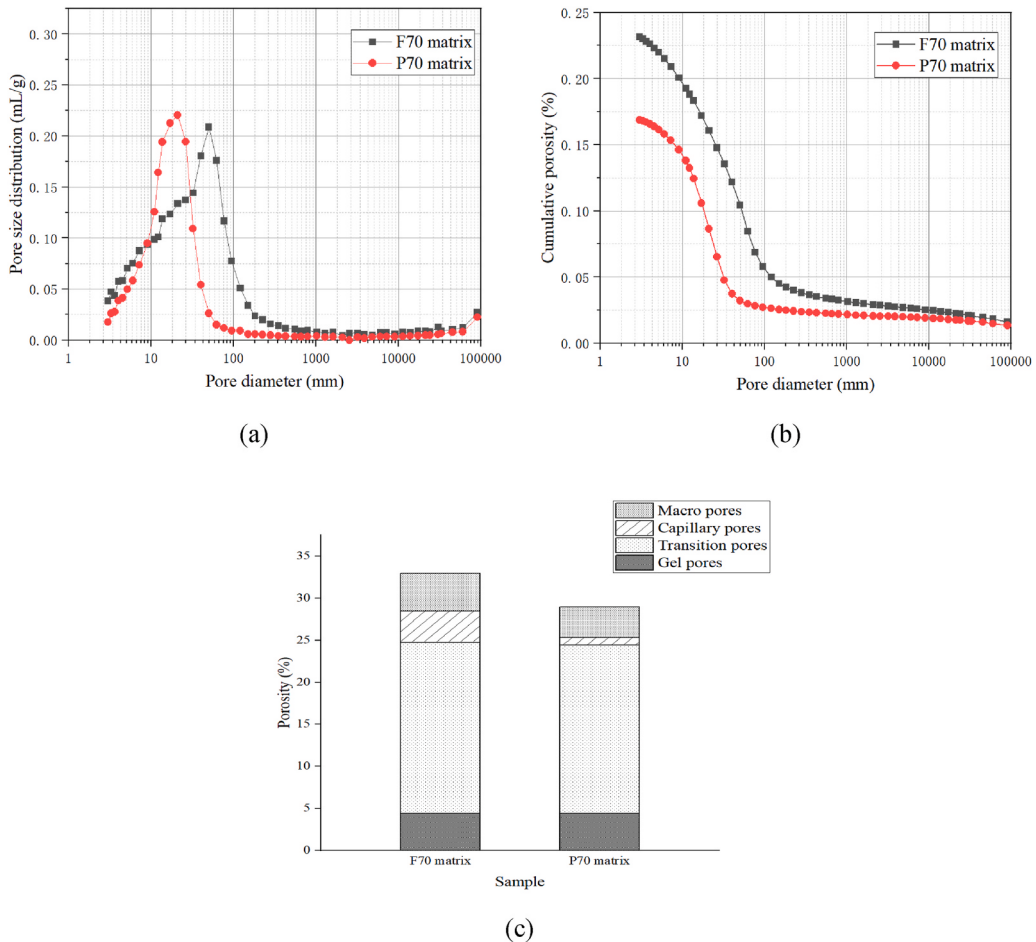


Fig. 15. Pore size distribution of each sample.

28 days of age are summarized in Table 8, and the tensile stress–strain curves are shown in Fig. 16. Before cracking, the ECC bore almost all loads by the matrix, and its variation in tensile strength was consistent with the obtained results on tensile strength, as discussed for CQM. As shown in the stress–strain curve, each obvious fluctuation indicates the formation of new cracks during loading. After the initial crack, the tensile load was mainly borne by the PVA fiber, and the deformation of the specimens increased significantly. Simultaneously, the stress quickly returned to its original level after an instant drop and continued to increase. As the strain increased, the above process was repeated many times, and dense and fine cracks formed on the specimen surface. When the external load reached its peak value, the specimen cracks no longer increased. Instead, the main crack was formed, the fiber at the main crack was pulled out, and the specimen was destroyed. The cracking patterns of the specimens are presented in Fig. 17. Dense and fine cracks were formed on the surface of F70. As the amount of CPBP used to replace fly ash increased, the number of cracks in the ECC decreased under the same stress level. As Fig. 17 shows, the tensile strength and elongation rate of the PVA fiber are 1560 MPa and 6.5%, respectively, whereas the tensile strains of FP35 and P70 in this test were less than

6.5%. When the load was stopped, the PVA fiber remained in the elastic stage. Owing to the fiber's bridging capacity, the cracks of the ECC rebound and shrink, resulting in inconspicuous cracks in FP35 and P70.

F70, FP35, and P70 showed significant strain-hardening behavior during tensile stress and achieved tensile strain capacities of 6.76%, 4.39%, and 4.15%, respectively. Owing to the bridging capacity of the PVA fibers in CQM, the ECC specimens exhibited significant strain-hardening behavior during tensile stress. As the CPBP content increased from 0% in F70 to 35% in FP35, the tensile strength of the ECC mix increased by 40.24%. From the results of the previous matrix test, it can be observed that CPBP as admixture enhances the strength of CQM, thereby increasing the initial cracking and ultimate strength of the ECC. However, when the CPBP content increased from 35% to 70%, the CQM tensile strength decreased by 12.22% owing to the joint filling effect of fly ash and CPBP, which have different particle shapes and fineness. As the matrix strength increases, the bond force between the matrix and the PVA fiber also increases, resulting in an increase in resistance to fiber slippage, which consequently limits the formation of multiple cracks and the strain capacity [60,61]. In general, when the cement content was fixed, the incorporation of CPBP effectively enhanced the tensile and compressive strength but reduced the ultimate tensile strain of the ECC specimen to a certain extent. Moreover, FP35 and P70 both meet the requirements of ECC materials for tensile properties. FP35 shows a better ultimate tensile strength (5.89 MPa) and strain capacity (4.39%). Zhao et al. [33] used ceramic powder as a supplementary cementing material to replace cement partially in PVA-ECC materials and showed that by maintaining the content of fly ash constant and using ceramic powder to replace part of the cement can effectively improve the ultimate tensile strength but weaken the tensile strength of the ECC specimen

Table 8
Uniaxial tensile test results of the ECC.

Sample	Initial cracking strength (MPa)	Initial cracking strain capacity (%)	Tensile strength (MPa)	Tensile strain capacity (%)
F70	2.42	0.32	4.20	6.76
FP35	3.14	0.03	5.89	4.39
P70	3.25	0.11	5.17	4.15

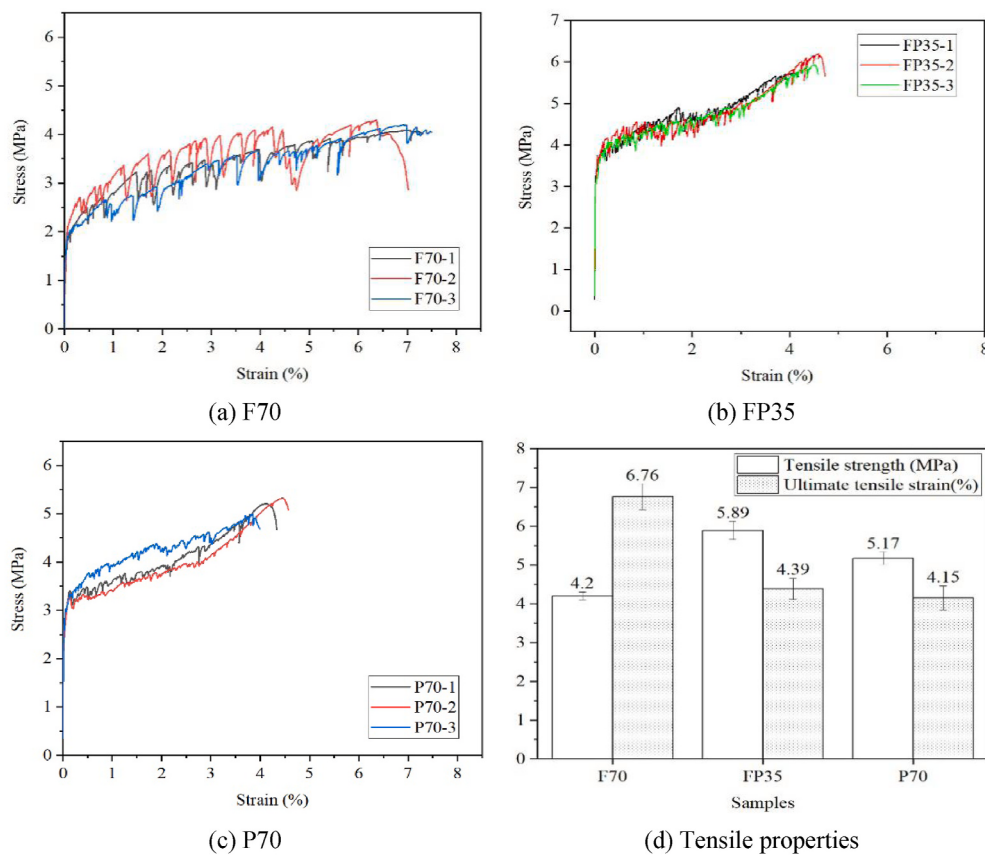


Fig. 16. Tensile stress–strain curves and tensile properties of ECC specimens at 28 days of age.

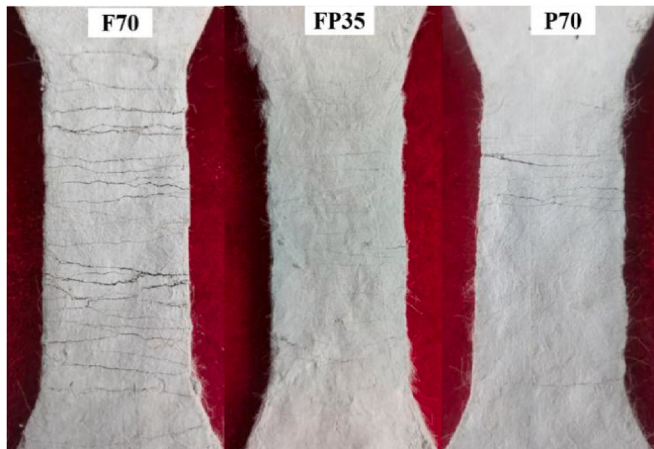


Fig. 17. Cracking patterns of specimens.

to a certain extent. The results of this experiment can be complementary to the research results of Zhao et al. [33] with respect to the macroscopic effects of cement, fly ash, and CPBP in ECC materials.

4. Conclusions

This study designed a new type of ECC, adding CPBP as a replacement for fly ash, which can realize the reutilization of ceramic waste and alleviate the high demand for high-quality fly ash. The ECC specimens containing CPBP as supplementary cementitious material exhibited significant strain-hardening behavior during tensile stress and achieved at least 4% ultimate tensile strain capacity. Therefore, it is feasible to use

CPBP as a fly ash replacement material to produce ECCs with acceptable performance. The main conclusions are as follows:

- 1) The 7-day activity index of CPBP was the same as that of fly ash, while the 28-day activity index of CPBP was 14.29% higher than that of fly ash. Regarding CPBP and fly ash as cementitious materials, under the condition of a constant water–binder ratio, the flexural and compressive strength of cement mortar decreased with the increase in CPBP and fly ash content as cement replacement. Furthermore, for the same amount of cement substitution, the compressive strength of cement-CPBP mortar was higher than that of fly ash mortar at 28 days. With the addition of CPBP from 0% to 50% of cement replacement, the fluidity of the mortar first increases and then decreases.
- 2) CQM exhibits obvious brittleness during uniaxial tensile and compressive loads. When CPBP replaces 35% of fly ash, the compressive and tensile strengths of CQM in this experiment were maximized, and simultaneously, the ultimate tensile strain of CQM was maintained at a considerable level.
- 3) At the age of 28 days, CQM with CPBP content had no calcium hydroxide peak but a calcium carbonate peak in the XRD pattern. The active SiO_2 in CPBP participates in hydration to produce more compounds that significantly contribute to the strength and benefits the CQM's early strength growth. Thus, CQM mixed with CPBP has a lower porosity than that of CQM with fly ash.
- 4) The addition of CPBP can significantly refine the pore structure of CQM. Within the range of CPBP content from 0% to 70%, the porosity and the most probable pore size of CQM decreased by 13.95% and 58.13%, respectively, which helped refine the CQM pore structure. Moreover, with the addition of CPBP, a dense CQM microstructure is achieved and the proportion of harmful pores is significantly reduced.

5) When the cement content is fixed, CPBP as a substitute for fly ash can effectively increase the initial and ultimate tensile strengths of the ECC but reduce its ultimate tensile strain capacity. As the CPBP content in cementitious materials increases, the ECC ultimate tensile capacity and the number of cracks in the ECC continued to decrease, while the tensile strength first increased and then decreased. Regardless of whether CPBP replaces half or all fly ash, the new designed ECC can achieve good tensile properties, which provides it with great engineering application prospects. Furthermore, when the CPBP content was 35%, the designed ECC showed a better ultimate tensile strength (5.89 MPa) and strain capacity (4.39%).

Credit author statement

Yan Xiong: Conceptualization, Methodology, Funding acquisition, Resources, Investigation, Writing – review & editing. Guozhong Xu: Investigation, Data curation, Writing – original draft. Di Wu: Conceptualization, Investigation, Writing – review & editing. Shuai Fang: Investigation, Data curation. Yingfeng Tang: Investigation.

Declaration of competing interest

The authors declare that they have no known competing financial interests or personal relationships that could have appeared to influence the work reported in this paper.

Acknowledgements

The authors would like to acknowledge the funding provided by National Natural Science Foundation of China (51878298, 51778160), Natural Science Foundation of Guangdong Province of China (2021A1515012606), Science and Technology Program of Guangdong Province of China (2018B02028003) and State Key Laboratory of Sub-tropical Building Science International Cooperation Open Project of China (2019ZA05).

References

- [1] C.L. Hwang, M.D. Yehualaw, D.H. Vo, T.P. Huynh, Development of high-strength alkali-activated pastes containing high volumes of waste brick and ceramic powders, *Construct. Build. Mater.* 218 (2019) 519–529, <https://doi.org/10.1016/j.conbuildmat.2019.05.143>.
- [2] N. Ay, M. Ünal, The use of waste ceramic tile in cement production, *Cement Concr. Res.* 30 (3) (2000) 497–499, [https://doi.org/10.1016/S0008-8846\(00\)00202-7](https://doi.org/10.1016/S0008-8846(00)00202-7).
- [3] R.M. Senthamarai, P.D. Manoharan, Concrete with ceramic waste aggregate, *Cement Concr. Compos.* 27 (9–10) (2005) 910–913, <https://doi.org/10.1016/j.cemconcomp.2005.04.003>.
- [4] F.Pacheco-Torgal, Y. Ding (Eds.), *Handbook of Recycled Concrete and Demolition Waste*, Elsevier, 2013.
- [5] D. Wattanasiriwech, A. Saiton, S. Wattanasiriwech, Paving blocks from ceramic tile production waste, *J. Clean. Prod.* 17 (18) (2009) 1663–1668, <https://doi.org/10.1016/j.jclepro.2009.08.008>.
- [6] Y. Huang, J. Luo, B. Xia, Application of cleaner production as an important sustainable strategy in the ceramic tile plant—a case study in Guangzhou, China, *J. Clean. Prod.* 43 (2013) 113–121, <https://doi.org/10.1016/j.jclepro.2012.12.013>.
- [7] P.O. Awoyerwa, J.O. Akinmusuru, A.R. Dawson, J.M. Ndambuki, N.H. Thom, Microstructural characteristics, porosity and strength development in ceramic-laterized concrete, *Cement Concr. Compos.* 86 (2018) 224–237, <https://doi.org/10.1016/j.cemconcomp.2017.11.017>.
- [8] S. Siddique, S. Chaudhary, S. Shrivastava, T. Gupta, Sustainable utilisation of ceramic waste in concrete: Exposure to adverse conditions, *J. Clean. Prod.* 210 (2019) 246–255, <https://doi.org/10.1016/j.jclepro.2018.10.231>.
- [9] S.H. Wang, C. Wang, Y.Q. Wang, X.Z. Zhang, Y.N. Chen, Production and reutilization of ceramic waste, *Journal of Ceramics* 40 (2019) 710–717, <https://doi.org/10.13957/j.cnki.txcb.2019.06.002>, 06.
- [10] P. Giacomini, World production and consumption of ceramic tiles, *Ceramic World Review* 85 (2018) 54–62.
- [11] M. Samadi, G.F. Huseien, H. Mohammadhosseini, H.S. Lee, N.H.A.S. Lim, M. M. Tahir, R. Alyousef, Waste ceramic as low cost and eco-friendly materials in the production of sustainable mortars, *J. Clean. Prod.* 266 (2020), <https://doi.org/10.1016/j.jclepro.2020.121825>, 121825.
- [12] R.M. Senthamarai, P.D. Manoharan, Concrete with ceramic waste aggregate, *Cement Concr. Compos.* 27 (9–10) (2005) 910–913, <https://doi.org/10.1016/j.cemconcomp.2005.04.003>.
- [13] X.F. Luan, Y.N. Cao, L.H. Xiao, H.J. Peng, Y.Q. Xie, Progress in application of ceramic waste in building materials, *Mater. Rev.* 29 (13) (2015) 145–150, <https://doi.org/10.11896/j.issn.1005-023X.2015.013.028>.
- [14] G.X. Wang, L. Tan, Y.H. Nie, X. Tian, Progress in application of ceramic waste in building materials, *Mater. Rev.* 31 (2012) 1564–1570, <https://doi.org/10.16552/j.cnki.issn1001-1625.2012.06.012>, 06.
- [15] L.X. Li, Y.Q. Wang, Y.X. Han, S.L. Bao, Utilizing ceramic waste as a construction material, *J. Northeast. Univ. (Nat. Sci.)* 32 (2011) 419–422, <https://doi.org/10.3969/j.issn.1005-3026.2011.03.029>, 03.
- [16] P. Torkittikul, A. Chaipanich, Utilization of ceramic waste as fine aggregate within Portland cement and fly ash concretes, *Cement Concr. Compos.* 32 (6) (2010) 440–449, <https://doi.org/10.1016/j.cemconcomp.2010.02.004>.
- [17] A.V. Alves, T.F. Vieira, J. De Brito, J.R. Correia, Mechanical properties of structural concrete with fine recycled ceramic aggregates, *Construct. Build. Mater.* 64 (2014) 103–113, <https://doi.org/10.1016/j.conbuildmat.2014.04.037>.
- [18] S. Subaşı, H. Öztürk, M. Emiroğlu, Utilizing of waste ceramic powders as filler material in self-consolidating concrete, *Construct. Build. Mater.* 149 (2017) 567–574, <https://doi.org/10.1016/j.conbuildmat.2017.05.180>.
- [19] M. Samadi, G.F. Huseien, H. Mohammadhosseini, H.S. Lee, N.H.A.S. Lim, M. M. Tahir, R. Alyousef, Waste ceramic as low cost and eco-friendly materials in the production of sustainable mortars, *J. Clean. Prod.* 266 (2020), <https://doi.org/10.1016/j.jclepro.2020.121825>, 121825.
- [20] L.X. Li, Study on the application of the ceramic waste powder in concrete, *Journal of Ceramics* 31 (2010) 270–274, <https://doi.org/10.13957/j.cnki.txcb.2010.02.035>, 02.
- [21] L.R. Steiner, A.M. Bernardin, F. Pelisser, Effectiveness of ceramic tile polishing residues as supplementary cementitious materials for cement mortars, *Sustainable Materials and Technologies* 4 (2015) 30–35, <https://doi.org/10.1016/j.susmat.2015.05.001>.
- [22] L.G. Li, Z.Y. Zhuo, J. Zhu, J.J. Chen, A.K.H. Kwan, Reutilizing ceramic polishing waste as powder filler in mortar to reduce cement content by 33% and increase strength by 85%, *Powder Technol.* 355 (2019) 119–126, <https://doi.org/10.1016/j.powtec.2019.07.043>.
- [23] L.G. Li, Z.Y. Zhuo, A.K.H. Kwan, T.S. Zhang, D.G. Lu, Cementing efficiency factors of ceramic polishing residue in compressive strength and chloride resistance of mortar, *Powder Technol.* 367 (2020) 163–171, <https://doi.org/10.1016/j.powtec.2020.03.050>.
- [24] V.C. Li, Engineered cementitious composites - tailored composites through micromechanical modeling, *J. Adv. Concr. Technol.* 1 (3) (1998).
- [25] V.C. Li, S. Wang, C. Wu, Tensile strain-hardening behavior of polyvinyl alcohol engineered cementitious composite (PVA-ECC), *ACI Materials Journal-American Concrete Institute* 98 (6) (2001) 483–492. <https://www.researchgate.net/publication/2798882>.
- [26] V.C. Li, *Progress and Applications of Engineered Cementitious Composites*, 2007.
- [27] Victor C. Li, On engineered cementitious composites (ECC) a review of the material and its applications, *J. Adv. Concr. Technol.* 1 (3) (2003) 215–230, <https://doi.org/10.3151/jact.1.215>.
- [28] T. Kanda, T. Saito, N. Sakata, M. Hiraishi, Tensile and anti-spalling properties of direct sprayed ECC, *J. Adv. Concr. Technol.* 1 (3) (2003) 269–282, <https://doi.org/10.3151/jact.1.269>.
- [29] V.C. Li, *High Performance Fiber Reinforced Cementitious Composites as Durable Material for Concrete Structure Repair*, 2004.
- [30] V.C. Li, Tailoring ECC for special attributes: a review, *International Journal of Concrete Structures and Materials* 6 (3) (2012) 135–144, <https://doi.org/10.1007/s40069-012-0018-8>.
- [31] K. Minoru, R. Keitetsu, Recent progress on HPFRCC in Japan required performance and applications, *J. Adv. Concr. Technol.* 4 (1) (2006) 19–33, <https://doi.org/10.3151/jact.4.19>.
- [32] M.D. Lepechi, V.C. Li, Application of ECC for bridge deck link slabs, *Mater. Struct.* 42 (9) (2009) 1185, <https://doi.org/10.1617/s11527-009-9544-5>.
- [33] J. Zhao, C. Yan, S. Liu, J. Zhang, S. Li, Y. Yan, Effect of solid waste ceramic on uniaxial tensile properties and thin plate bending properties of polyvinyl alcohol engineered cementitious composite, *J. Clean. Prod.* 268 (2020), <https://doi.org/10.1016/j.jclepro.2020.122329>, 122329.
- [34] Z. Pan, C. Wu, J. Liu, W. Wang, J. Liu, Study on mechanical properties of cost-effective polyvinyl alcohol engineered cementitious composites (PVA-ECC), *Construct. Build. Mater.* 78 (2015) 397–404, <https://doi.org/10.1016/j.conbuildmat.2014.12.071>.
- [35] S. Saha, C. Rajasankaran, Enhancement of the properties of fly ash based geopolymer paste by incorporating ground granulated blast furnace slag, *Construct. Build. Mater.* 146 (2017) 615–620, <https://doi.org/10.1016/j.conbuildmat.2017.04.139>.
- [36] Z. Zhang, J. Zhang, D.J. Ji, Optimization of mix proportion of ceramic polishing powder and fly ash codoped concrete, *J. Shandong Univ. Technol.* 32 (4) (2018) 40–44+49, <https://doi.org/10.13367/j.cnki.sdg.2018.04.008>.
- [37] Gbt 51003-2014, *Technical Code for Application of Mineral Admixture*, China Architecture and Building Press, Beijing, 2014 (in Chinese).
- [38] J. Zhang, H. Sun, Influence of Granulometry and Reactivity of mixing materials on the properties of mortar and concrete, *Journal of Anyang Institute of Technology* 18 (6) (2019) 37–41, <https://doi.org/10.19329/j.cnki.1673-2928.2019.06.010>.
- [39] Y. Li, R.Q. Liu, W.H. Qi, Y.H. Zhang, Effects of particle size distribution of silica fume on pore structure and compressive strength of concrete at low temperature,

- China Powder Sci. Technol. 25 (2019) 75–80, <https://doi.org/10.13732/j.issn.1008-5548.2019.06.013>, 06.
- [40] H.Q. Li, J.Z. Zheng, Effect of fly ash particle size and content on strength of high performance concrete, Northern Communications (2015) 22–25, <https://doi.org/10.15996/j.cnki.bfjt.2015.08.006>, 08.
- [41] Haifeng Qi, Comparative Study of Flowability of Coal Powders and Analysis of Relate Influence Factors (Doctoral Dissertation, East China University of Science and Technology, Shanghai, 2012).
- [42] Iso 13320-1-1999, Particle Size Analysis - Laser Diffraction Methods - Part 1: General Principles, Standardization Administration, China, 1999 (in Chinese).
- [43] Gbt 176-2017, Methods for Chemical Analysis of Cement, Standardization Administration, China, 2017 (in Chinese).
- [44] Gb175-2007, Common Portland Cement, Standardization Administration, China, 2007 (in Chinese).
- [45] Gbt 1596-2017, Fly Ash Used for Cement and Concrete, Standardization Administration, China, 2017 (in Chinese).
- [46] Gb/T 2419-2005, Test Method for Fluidity of Cement Mortar, Standardization Administration, Beijing: China, 2005 (in Chinese).
- [47] Gb/T17671-1999, Method of Testing Cements—Determination of Strength, Standardization Administration, China, 1999 (in Chinese).
- [48] ISO 679:2009, Cement - Test Methods - Determination of Strength.
- [49] E.H. Yang, V.C. Li, Tailoring engineered cementitious composites for impact resistance, Cement Concr. Res. 42 (8) (2012) 1066–1071, <https://doi.org/10.1016/j.cemconres.2012.04.006>.
- [50] S. Wang, V.C. Li, Engineered cementitious composites with high-volume fly ash, ACI Mater. J. 104 (3) (2007) 233.
- [51] F. Andreola, L. Barbieri, I. Lancellotti, M.C. Bignozzi, F. Sandrolini, New blended cement from polishing and glazing ceramic sludge, Int. J. Appl. Ceram. Technol. 7 (4) (2010) 546–555, <https://doi.org/10.1111/j.1744-7402.2009.02368.x>.
- [52] H. Yokota, K. Rokugo, N. Sakata, JSCE Recommendations for Design and Construction of High Performance Fiber Reinforced Cement Composite with Multiple Fine Cracks. High Performance Fiber Reinforced Cement Composites, Springer, Tokyo, Japan, 2008, https://doi.org/10.3151/coj1975.43.3_3.
- [53] Jct2461-2018. Standard Test Method for Mechanical Properties of Ductile Fiber Reinforced Cementitious Composites.
- [54] A.E.B. Cabral, V. Schalch, D.C.C. Dal Molin, J.L.D. Ribeiro, Mechanical properties modeling of recycled aggregate concrete, Construct. Build. Mater. 24 (4) (2010) 421–430, <https://doi.org/10.1016/j.conbuildmat.2009.10.011>.
- [55] G.X. Wang, D.G. Su, Y.X. Zhao, Fabrication of autoclaved silicate products with ceramic polishing powders as raw material, 07, J. S. China Univ. Technol. (2008) 124, <https://doi.org/10.3321/j.issn:1000-565X.2008.07.025>, 127+133.
- [56] G.X. Wang, L. Tan, Y.H. Nie, X. Tian, Effect of ceramic polishing powder on the chloride permeability of concrete, BULLETIN OF THE CHINESE CERAMIC SOCIETY 31 (2012) 1564–1570, <https://doi.org/10.16552/j.cnki.issn1001-1625.2012.06.012>, 06.
- [57] M. Şahmaran, E. Özbay, H.E. Yücel, M. Lachemi, V.C. Li, Effect of fly ash and PVA fiber on microstructural damage and residual properties of engineered cementitious composites exposed to high temperatures, J. Mater. Civ. Eng. 23 (12) (2011) 1735–1745, [https://doi.org/10.1061/\(ASCE\)MT.1943-5533.0000335](https://doi.org/10.1061/(ASCE)MT.1943-5533.0000335).
- [58] S. Cui, P. Liu, E. Cui, J. Su, B. Huang, Experimental study on mechanical property and pore structure of concrete for shotcrete use in a hot-dry environment of high geothermal tunnels, Construct. Build. Mater. 173 (2018) 124–135, <https://doi.org/10.1016/j.conbuildmat.2018.03.191>.
- [59] F.S. Rostasy, R. Weiß, G. Wiedemann, Changes of pore structure of cement mortars due to temperature, Cement Concr. Res. 10 (2) (1980) 157–164, [https://doi.org/10.1016/0008-8846\(80\)90072-1](https://doi.org/10.1016/0008-8846(80)90072-1).
- [60] C.L. Liu, Y.Z. Bi, Y. Hua, Mechanical properties of PVA-ECC with high volume fly ash and mechanism analysis of fly ash, BULLETIN OF THE CHINESE CERAMIC SOCIETY 36 (11) (2017) 3739–3744, <https://doi.org/10.16552/j.cnki.issn1001-1625.2017.11.027>.
- [61] C. Redon, V.C. Li, C. Wu, H. Hoshiro, T. Saito, A. Ogawa, Measuring and modifying interface properties of PVA fibers in ECC matrix, J. Mater. Civ. Eng. 13 (6) (2001) 399–406, [https://doi.org/10.1061/\(ASCE\)0899-1561\(2001\)13:6\(399\)](https://doi.org/10.1061/(ASCE)0899-1561(2001)13:6(399)).